Relating domain shape to growth velocity anisotropy: Inherent symmetry of the Wulff construction

Qi Jiang, Joseph E. Maclennan, and Noel A. Clark
Condensed Matter Laboratory, Department of Physics, University of Colorado, Boulder, Colorado 80309
(Received 22 October 1996)

The Wulff construction relates the equilibrium shape of a crystal to its anisotropic surface tension profile, and, in a formally equivalent way, relates the shape of an evolving domain to its anisotropic growth velocity profile. We demonstrate explicitly the underlying complementarity and symmetry between these real space shapes and their generating profiles. By exploiting this symmetry, we have developed a simplified method for determining velocity profiles from the shapes of growing domains, demonstrated here for polarization reversal domains in ferroelectric liquid crystals. [S1063-651X(97)12208-5]

PACS number(s): 61.30.Cz, 77.80.Fm, 83.70.Jr, 81.10.Aj

Domains in condensed phases can exhibit remarkable interface structures with characteristic morphologies and complex evolutionary motion [1–9]. The modeling of domain shape requires the calculation of a $(D-1)$-dimensional interface profile in a D-dimensional space, and is typically a complex nonlinear and nonlocal problem. The equations describing moving domain boundaries are generally so complicated that not only is analytic computation difficult, but even numerical solutions are limited to special cases. For these reasons much attention has been paid to seeking analytical methods effective for specific physical systems, such as the Wulff construction, a simple geometrical prescription for determining the equilibrium shape of single crystals from their anisotropic surface energy density [10].

An important class of domain formation problems relates to the reversal of magnetization in ferromagnets and of polarization in ferroelectric materials. Field-driven reversal is in general mediated by the formation of domains and the motion of domain walls, processes that determine important device parameters such as hysteresis and switching time. A particularly interesting example of such domain-mediated switching is found in electric field-induced polarization reversal in surface stabilized ferroelectric liquid crystals (SSFLCs) [11,12]. The SSFLC domains have a remarkable, highly anisotropic, characteristic ''speedboat'' shape [13,14], as shown in Fig. 1. These domains, which nucleated from impurity particles (indicated in one domain by an arrow), evidently grow only slowly to the left but rapidly to the right, and are characterized by shape singularities in the form of sharp corners and almost flat sides. Despite such exotic shapes, some aspects of the growth dynamics of SSFLC polarization reversal domains are quite simple: at a fixed value of all but the weakest applied fields, the domains grow from their nucleation site at a constant rate and in a self-similar way, i.e., their shape remains the same and their linear dimensions increase in time at a constant rate [15]. We refer to this as constant-rate self-similar growth (CRSSG), and the discussion in this paper is limited to this case. Under conditions of CRSSG, the two-dimensional (2D) domain shape and growth rate are entirely determined by the anisotropic local domain wall velocity $v_n(\hat{\mathbf{n}},E)\hat{\mathbf{n}}$, which is equivalent to the velocity, in an electric field E, of an infinite planar (1D) domain wall normal to $\hat{\mathbf{n}}=\cos\phi\hat{\mathbf{x}}+\sin\phi\hat{\mathbf{y}}$. A basic prerequisite in analyzing such domains is developing useful relationships between the velocity profile $v_n(\phi)$, the quantity most readily obtained from models, and the domain shape, the quantity most readily evaluated from experiment, described by the anisotropic radius $\mathbf{r}(\theta)$ measured from the nucleation site as a function of polar angle θ.

The connection between growing domain shape and anisotropic velocity profile was first explored by Frank. Under the assumption that the growth velocity depends only on the local orientation of the interface, Frank showed that the domain shape can be obtained from the inverse velocity profile $1/v_n(\hat{\mathbf{n}})\hat{\mathbf{n}}$ [16]. Since that time, the formal equivalence of the Wulff construction for equilibrium crystal shapes to Frank's ''slowness vector'' method has been realized, and a variety of geometrical and mathematical methods for computing domain growth from velocity profile have been developed, including nine distinct approaches reviewed in [17–19] and the references therein.

Previously, we simulated 2D domain growth in FLCs numerically, comparing the computed shapes to those obtained using a Wulff construction with 1D velocity profiles generated from an FLC model system [20,21]. Although anisotropic domain shapes were obtained, the pointed bow-flat

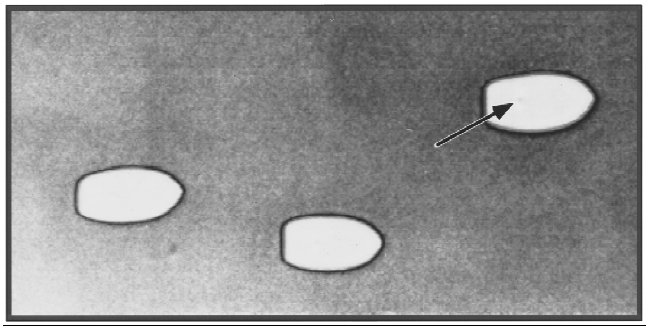

FIG. 1. Polarization domains in an SSFLC cell. The domains nucleate from impurities (indicated in one domain by an arrow) and grow self-similarly, with a characteristic ''speedboat'' shape. The cell is 4 μm thick and contains the Merck ferroelectric liquid crystal mixture ZLI-3654 ($E=60$ mV/μm, $T=50\,^{\circ}$C). The horizontal dimension is about 300 μm.

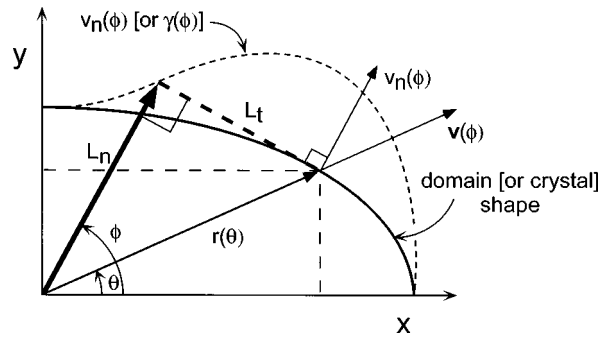

FIG. 2. Geometry of domain shape (or Wulff construction) calculations. The curved domain boundary advances with velocity **v**, the normal and transverse components of the radius vector $\mathbf{r}(\theta)$ being given respectively by L_n and L_t. L_n is proportional to $v_n(\phi)$ for constant-rate self-similar domain growth [or to $\gamma(\phi)$ in equilibrium crystals].

stern anisotropy characteristic of speedboats was not found. This led us to explore means of extracting the velocity profile directly from the boat shape, and thus to the method described here.

In this paper we present a simple and elegant derivation of the relationship between real space shapes and their generating profiles that makes explicit the inherent symmetry in the shape-to-profile transformations and their inverses, and demonstrates the complementary nature of these two representations. The formalism is applied to the determination of velocity growth profiles from the shapes of polarization switching domains undergoing CRSSG in SSFLC cells. We also establish conditions of $v_n(\hat{\mathbf{n}})$ that lead to characteristic structural features of domains such as facets and cusps.

The Wulff construction is an appealingly straightforward geometrical method for obtaining the equilibrium shape of a crystal from its (generally anisotropic) local surface energy density $\gamma(\hat{\mathbf{n}})$, where $\hat{\mathbf{n}}$ is the local normal to the crystal surface. In the 2D case of interest here, the crystal shape $r(\theta)$ corresponds geometrically to the region in real space that lies within the set of dashed lines (see Fig. 2) drawn through each point of the curve $L_n(\phi) \propto \gamma(\phi)$ such that each line is normal to the radial vector $L_n(\phi)\hat{\mathbf{n}}$ [22]. The resulting shape is that which minimizes the net surface energy F of a 2D crystal domain with fixed area, written as

$$F = \oint \gamma(\phi) ds - p \int dA. \tag{1}$$

Here $\gamma(\phi)$ is the surface tension, which is only dependent on the normal angle ϕ, ds is an infinitesimal element of arclength along the boundary, and p is a Lagrange multiplier. Using differential geometry, we can recast this in the form

$$F = \int_0^1 [2\pi\gamma(\alpha)/\kappa - (p/2)\mathbf{r}\times\mathbf{r}_\alpha] d\alpha, \tag{2}$$

where the parameter $\alpha = \phi/2\pi$. The curvature $\kappa = \mathbf{r}_\alpha \times \mathbf{r}_{\alpha\alpha}/\sqrt{(\mathbf{r}_\alpha \cdot \mathbf{r}_\alpha)^3}$, with $\mathbf{r}_\alpha = d\mathbf{r}/d\alpha$, and the area $A = (1/2)\int \mathbf{r}\times\mathbf{r}_\alpha \, d\alpha$. The crystal shape is found by minimizing F with respect to $\mathbf{r}(\theta)$. After applying the Frenet-Serret equations ($\partial\mathbf{t}/\partial s = -\kappa\mathbf{n}$ and $\partial\mathbf{n}/\partial s = \kappa\mathbf{t}$, where **t** and **n** are the unit vectors respectively normal and tangent to the surface), we obtain the following basic equations, showing that $r(\theta)$ and $\gamma(\phi)$ are transform pairs:

$$\kappa = \frac{1}{R} = p \Big/ \left[\gamma(\phi) + \frac{d^2\gamma(\phi)}{d\phi^2} \right], \tag{3a}$$

$$\kappa_\gamma = \frac{1}{\Gamma} = (1/p) \Big/ \left\{ r(\theta)\cos^2(\phi-\theta) + \frac{d^2}{d\beta^2}[r(\theta)\cos^2(\phi-\theta)] \right\}, \tag{3b}$$

$$\frac{d[\ln r(\theta)]}{d\theta} = \frac{d[\ln\gamma(\phi)]}{d\phi} = -\tan(\phi-\theta), \tag{3c}$$

where p may be thought of as a surface pressure, and $\beta = 2\phi - \theta$.

The complementarity of the Wulff construction and its inverse was recognized by Herring [22] and by Andreev [23], who pointed out that the free energy and the crystal shape are related by a Legendre transformation (see the review by Wortis [24]). The explicit form of Eq. (3c) of our derivation, is however, new: it exhibits the underlying symmetry between $r(\theta)$ and $\gamma(\phi)$ and enables the mathematical transformation between these two complementary representations. The respective radii of curvature $R(\theta)$ of the crystal and $\Gamma(\phi)$ of the surface tension profile are given by the general formulas:

$$\kappa = \frac{1}{R} = \left(\frac{dx}{d\phi}\frac{d^2y}{d\phi^2} - \frac{d^2x}{d\phi^2}\frac{dy}{d\phi} \right) \Big/ \left[\left(\frac{dx}{d\phi}\right)^2 + \left(\frac{dy}{d\phi}\right)^2 \right]^{3/2}, \tag{4a}$$

$$\kappa_\gamma = \frac{1}{\Gamma} = \left(\frac{d\gamma_x}{d\phi}\frac{d^2\gamma_y}{d\phi^2} - \frac{d^2\gamma_x}{d\phi^2}\frac{d\gamma_y}{d\phi} \right) \Big/ \left[\left(\frac{d\gamma_x}{d\phi}\right)^2 + \left(\frac{d\gamma_y}{d\phi}\right)^2 \right]^{3/2}, \tag{4b}$$

where the surface tension has been expressed in component form, $\gamma(\phi)\hat{\mathbf{n}} = \gamma_x\hat{\mathbf{x}} + \gamma_y\hat{\mathbf{y}}$.

In the model for CRSSG domain growth, the domain boundary is represented by a closed curve in 2D specified by $\mathbf{r}(t) = x(t)\hat{\mathbf{x}} + y(t)\hat{\mathbf{y}}$, as shown schematically in Fig. 2. For CRSSG, equations analogous to Eqs. (3) relate the velocity profile $v_n(\phi)$ to the domain shape at long times (when the domain has become much larger than its starting size):

$$\kappa = \frac{1}{R} = (1/t) \Big/ \left[v_n(\phi) + \frac{d^2 v_n(\phi)}{d\phi^2} \right], \tag{5a}$$

$$\kappa_v = \frac{1}{V} = t \Big/ \left\{ r(\theta)\cos^2(\phi-\theta) + \frac{d^2}{d\beta^2}[r(\theta)\cos^2(\phi-\theta)] \right\}, \tag{5b}$$

$$\frac{d[\ln r(\theta)]}{d\theta} = \frac{d[\ln v_n(\phi)]}{d\phi} = -\tan(\phi-\theta). \tag{5c}$$

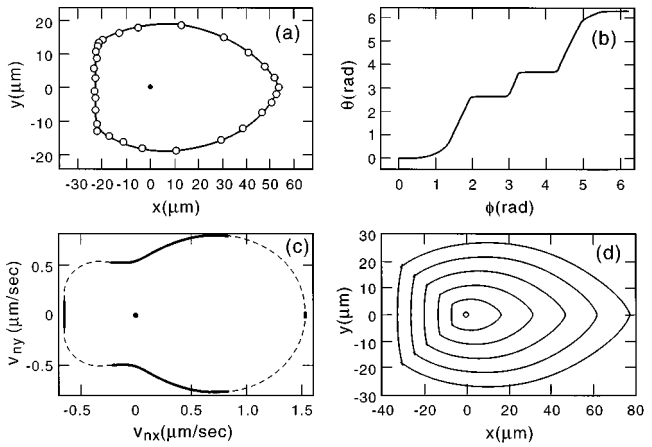

FIG. 3. Analysis of SSFLC domain growth. (a) Steady-state ''speedboat'' domain in the same cell as Fig. 1 with $E=25$ mV/μm. The dotted line corresponds to the experimental domain boundary, while the solid curve is a fit using polynomials. (b) Variation of polar angle θ with surface normal angle ϕ for the domain in (a). (c) Normal velocity profile $v_n(\phi)$ as a function of normal angle ϕ for the domain in (a). (d) Predicted growth of an initially circular domain at different times ($\Delta t=10$ ms) using the velocity profile shown in (c).

The velocity profile curvature, κ_v, is also given by an expression analogous to Eq. (4b).

In the CRSSG limit, which is reached very quickly in FLC cells, the geometric properties of the shape, which may include facets and cusps, are determined only by the normal velocity profile, $v_n(\phi)$. Previous analyses [17,20,21] have shown that for growth under conditions of constant domain wall velocity $v_n(\phi)$, starting from a domain of initial shape $\mathbf{r_0}(\theta)$, with $\mathbf{r_0}(\theta)=L_n^0(\theta)\hat{\mathbf{n}}+L_t^0(\theta)\hat{\mathbf{t}}$ using the geometry of Fig. 2, the evolution of the boundary is given by

$$x=[v_n(\phi)t+L_n^0(\phi)]\cos\phi-\left[\frac{dv_n(\phi)}{d\phi}t+L_t^0(\phi)\right]\sin\phi, \tag{6a}$$

$$y=[v_n(\phi)t+L_n^0(\phi)]\sin\phi+\left[\frac{dv_n(\phi)}{d\phi}t+L_t^0(\phi)\right]\cos\phi, \tag{6b}$$

where the tangential velocity component $v_t=dv_n/d\phi$.

The formal analogy between equilibrium crystal shapes and CRSSG domain shape is completed by noting that the functional analog to F in Eq. (1) is the power dissipation D accompanying domain motion

$$D(t)=2PE\int v_n(\hat{\mathbf{n}})ds-\frac{p'}{t^2}\int dA, \tag{7}$$

where $2P$ is the net polarization per unit area switched by passage of the domain wall, and p' is a Lagrange multiplier. The analogy, which illustrates that the domain shape adopted is that which minimizes D, also aids in picturing qualitatively the origin of the domain shape arising from the Wulff construction. This is seen in Fig. 2 to be the shape that results if each surface element maintains its orientation while

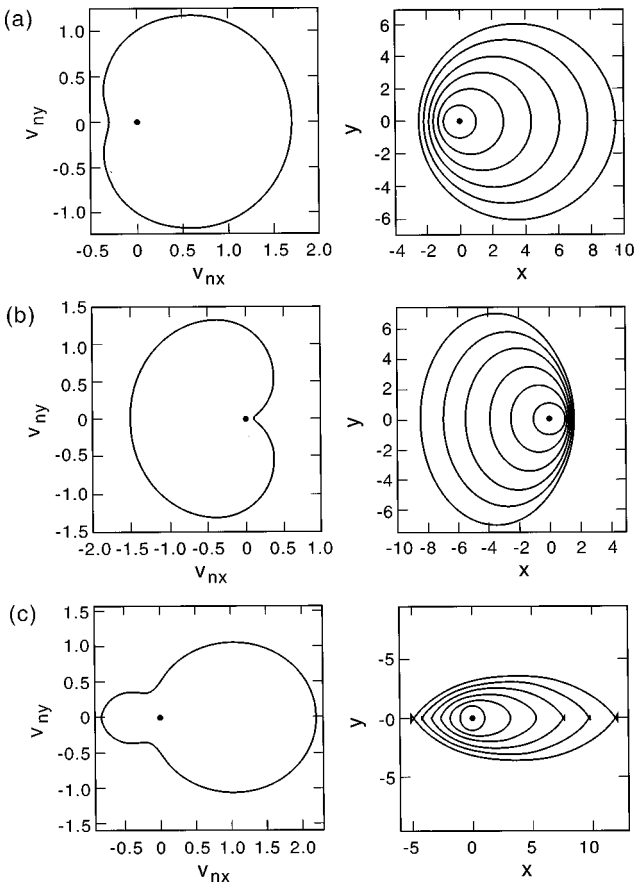

FIG. 4. Evolution of domain shape with time for different velocity profiles $v_n(\phi)=a_0+a_1\cos\phi+a_2\cos2\phi$. The velocity profiles are shown on the left, and the domain shapes, at unit time intervals, on the right. The initial domain shape is in each case a unit circle. (a) $a_0=1$, $a_1=0.7$, and $a_2=0$. Changing the sign of a_1 results in growth that is faster along $-x$. This form of $v_n(\phi)$ does not produce cusps. (b) $a_1=-0.7$, $a_2=-0.2$; (c) $a_1=0.7$, $a_2=0.5$. Cusps only develop in (c).

translating in its normal direction a distance $v_n(\phi)t$ and transversely a distance $v_t(\phi)t$ during the interval t.

The basic motivation for this work is to develop methods for extracting the velocity profile $v_n(\phi)$ from the domain shape $r(\theta)$, since it is $v_n(\phi)$ that is most readily obtained from microscopic or hydrodynamic models of the dynamics of the switching medium. The procedure followed here is to exploit the symmetry between $r(\theta)$ and $v_n(\phi)$ in Eqs. (5), applying Eq. (5c) twice, first to obtain $\phi(\theta)$ from $r(\theta)$, and then to use $\theta(\phi)$ to calculate $v_n(\phi)$. In the experiment, polarization reversal domains such as those in Fig. 1 are video recorded and their boundaries found via digital image processing, resulting in data of the kind shown in Fig. 3(a). The boundary is divided into three distinct curved segments, each of which is then fitted to a polynomial of the minimal order necessary to give a good representation (in this case second order for the stern and fifth order for the sides). The result is an analytical domain shape sufficiently smooth to extract $\phi(\theta)$, which is calculated by numerical integration with the result shown in Fig. 3(b). The corners, where ϕ jumps through large angles with little change in θ, cannot be resolved in the experiments, and so $\phi(\theta)$ is simply linearly interpolated between the limiting values of wall orientation

as the corner is approached from opposite directions. Finally, $\theta(\phi)$ is inserted in Eq. (5b), which can then be numerically integrated to obtain $v_n(\phi)$, shown in Fig. 3(c). Here the solid regions of $v_n(\phi)$ determine the evolution of the curved facets while the dashed regions correspond to the corners and are nonphysical. This procedure can be inverted by employing Eqs. (6a) and (6b) with $v_n(\phi)$ from Fig. 3(c). This yields the experimental shape at arbitrary times, as shown in Fig. 3(d) where the growth was started from a small circular domain. The main result of this analysis is the physical (solid) portions of $v_n(\phi)$ in Figure 3(c), which are available for comparison with the results of possible models.

The characteristic flattened stern and pointed bows of the SSFLC domains provide motivation to explore analytically the conditions under which facets and cusps appear in the domain shape. If we consider Eq. (5a), we see that an isotropic $v_n(\phi)$, for which $d^2v_n(\phi)/d\phi^2=0$, generates circular domains. If $v_n(\phi)$ is made anisotropic, then $d^2v_n(\phi)/d\phi^2$ becomes an oscillatory function of ϕ and $r(\theta)$ is modulated. Cusps [θ regions where $R(\theta)\rightarrow 0$] will form near ϕ values satisfying

$$v_n(\phi)+d^2v_n(\phi)/d\phi^2\leqslant 0 \tag{8}$$

if the anisotropy of $v_n(\phi)$ is large enough for this to occur. In order to explore the appearance of cusps, we express an anisotropic $v_n(\phi)$ as a Fourier series $v_n(\phi)=\Sigma_m a_m \cos m\phi$. The cases of nonzero first and second harmonics are presented explicitly as follows:

Case (1): $v_n(\phi)=a_0+a_1\cos\phi$. Adding a single harmonic leaves the circular domain shape unchanged, but causes the center of the circle to shift with time, as shown in Fig. 4(a). Cusps never occur in this case. An analogous result was found by Rudnick [4], who confirmed that this form of the surface tension produces no anisotropy in the shapes of domains in Langmuir films.

Case (2): $v_n(\phi)=a_0+a_1\cos\phi+a_2\cos 2\phi$. Substituting this normal velocity into Eq. (8) yields

$$\cos^2\phi\geqslant 1/2+(1/6)a_0/a_2, \tag{9}$$

independent of the coefficient a_1. This expression implicitly defines the location of a pair of singularities (''double points'') at which the domain boundary will be cusped. In all of these cases, a_0 is positive, or the domain would collapse, while a_1 and a_2 can have either sign. Equation (9) has a solution only if a_0/a_2 is in the range $-3\leqslant a_0/a_2\leqslant 3$. Outside this range, the singular points disappear. Numerical calculations confirm that the occurrence of the singular points is independent of the coefficient a_1. If we choose $a_0/a_2=-5$, we see from Fig. 4(a) that the domain does not develop any cusps, whereas in Fig. 4(b), where $a_0/a_2=2$, after a certain time two cusps appear along the x axis as expected. The positions of the cusps depend on the sign of a_2. For example, if $a_2<0$ then the cusps are located along the y axis. Note that in cases where there are cusps, the function $\phi(\theta)$ is discontinuous and $v_n(\phi)$ is not physically relevant over the jumps in ϕ [i.e., over the range specified by Eq. (8)]. Similar stability analyses for comparably simple model surface tension profiles also appear in the literature (see, for example, [17]).

In summary, we have developed a Wulff construction formalism for determining the evolution of two-dimensional domains based on their steady-state normal velocity profiles. The analysis highlights the complementarity of the real space domain shapes and their generating profiles, for both equilibrium crystals and growing domains. Our technique, in common with other Wulff velocity methods, yields such steady-state features as facets and cusps, but avoids the disadvantages and complexity of many of the earlier published procedures.

We wish to thank N. Lallemand and F. Durringer for their help in obtaining images of speedboats. This work was supported by NSF Grants No. EEC 90-15128 and No. DMR 92-24168, and by ARO Contract No. DAA H04-93-G0164.

[1] J. S. Langer, Rev. Mod. Phys. **52**, 1 (1980).
[2] J. S. Langer, in *Chance and Matter*, Les Houches Sessions XLVI, edited J. Souletie *et al.* (Elsevier, New York, 1987).
[3] M. Seul and D. Andelmann, Science **267**, 476 (1995).
[4] J. Rudnick and R. Bruinsma, Phys. Rev. Lett. **74**, 2491 (1995).
[5] S. Riviere and J. Meunier, Phys. Rev. Lett. **74**, 2495 (1995).
[6] J. B. Fournier, Phys. Rev. Lett. **75**, 854 (1995).
[7] P. Galatola and J. B. Fournier, Phys. Rev. Lett. **75**, 3297 (1995).
[8] R. C. Brower, D. A. Kessler, J. Koplik, and H. Levine, Phys. Rev. A **29**, 1335 (1984).
[9] T. M. Fischer, R. F. Bruinsma, and C. M. Knobler, Phys. Rev. E **50**, 413 (1995).
[10] G. Wulff, Z. Kristallogr. **34**, 449 (1901).
[11] N. A. Clark and S. T. Lagerwall, Appl. Phys. Lett. **36**, 899 (1980).
[12] M. A. Handschy and N. A. Clark, Ferroelectrics **59**, 69 (1984).
[13] M. A. Handschy and N. A. Clark, Appl. Phys. Lett. **41**, 39 (1982).
[14] Y. Ouchi, H. Takezoe, and A. Fukuda, Jpn. J. Appl. Phys. **126**, 1 (1987); Y. Ouchi, H. Takano, H. Takezoe, and A. Fukuda, *ibid.* **27**, 1 (1988); N. Hiji, Y. Ouchi, H. Takezoe, and A. Fukuda, *ibid.* **27**, L1 (1988).
[15] J. Z. Xue and N. A. Clark, Phys. Rev. E **48**, 2043 (1993).
[16] F. C. Frank, in *Growth and Perfection in Crystals*, edited by R. H. Doremus, B. W. Roberts, and D. Turnbull (Wiley, New York, 1958), pp. 411–419; F. C. Frank, Z. Phys. Chem. (Leipzig) **77**, 84 (1972).
[17] J. W. Cahn and W. C. Carter, Metall. Trans. A **27**, 1431 (1996).
[18] J. E. Taylor, J. W. Cahn, and C. A. Handwerker, Acta Metall. Mater. **40**, 1443 (1992).
[19] W. C. Carter and C. A. Handwerker, Acta Metall. Mater. **41**, 1633 (1993).
[20] J. E. Maclennan, Q. Jiang, and N. A. Clark, Phys. Rev. E **52**, 3904 (1995).

[21] Q. Jiang, J. E. Maclennan, and N. A. Clark, Phys. Rev. E **53**, 6074 (1996).

[22] C. Herring, Phys. Rev. **82**, 87 (1951); C. Herring, in *Structure and Properties of Solid Surfaces*, edited by R. Gomer and C. Smith (University of Chicago Press, Chicago, 1953).

[23] A. F. Andreev, Zh. Éksp. Teor. Fiz. **80**, 2042 (1981) [Sov. Phys. JETP **53**, 1063 (1981)].

[24] M. Wortis, in *Chemistry and Physics of Solid Surfaces VII*, edited by R. Vanselow and R. F. Howe (Springer-Verlag, Berlin, 1988).